

This item is the archived peer-reviewed author-version of:

Hierarchical $CdS/m - TiO_2/G$ ternary photocatalyst for highly active visible light-induced hydrogen production from water splitting with high stability

Reference:

Lu Yi, Cheng Xiu, Tian Ge, Zhao Heng, He Li, Hu Jie, Wu Si-Ming, Dong Ying, Chang Gang-Gang, Lenaerts Silvia,- Hierarchical $CdS/m - TiO_2/G$ ternary photocatalyst for highly active visible light-induced hydrogen production from water splitting with high stability
Nano energy - ISSN 2211-2855 - 47(2018), p. 8-17
Full text (Publisher's DOI): <https://doi.org/10.1016/J.NANOEN.2018.02.021>
To cite this reference: <http://hdl.handle.net/10067/1507200151162165141>

Hierarchical CdS/m-TiO₂/G Ternary Photocatalyst for Highly Active Visible Light-induced Hydrogen Production from Water Splitting with High Stability

Yi Lu,^a Xiu Cheng,^a Ge Tian,^a Heng Zhao,^a Li He,^a Jie Hu,^a Si-Ming Wu,^a Ying Dong,^a Gang-Gang Chang,^a Silvia Lenaerts,^b Stéphane Siffert,^c Gustaaf Van Tendeloo,^d Zhao-Fei Li,^e Ling-Ling Xu,^f Xiao-Yu Yang^{a, *} and Bao-Lian Su^{a, g, *}

^a *State Key Laboratory of Advanced Technology for Materials Synthesis and Processing, Wuhan University of Technology, 122, Luoshi Road, 430070, Wuhan, Hubei, China.*

^b *Research Group of Sustainable Energy and Air Purification (DuEL), Department of Bioscience Engineering, University of Antwerp, Antwerp, Belgium*

^c *Unité de Chimie Environnementale et Interactions sur le Vivant (UCEIV) - Université Littoral Côte d'Opale, 145 Avenue Maurice Schuman, 59140 Dunkerque, France*

^d *EMAT (Electron Microscopy for Materials Science), University of Antwerp, Groenenborgerlaan 171, B-2020 Antwerpen, Belgium*

^e *Petrochemical Research Institute of PetroChina, Beijing, 102206, P. R. China*

^f *National Center for Magnetic Resonance in Wuhan, State Key Laboratory of Magnetic Resonance and Atomic and Molecular Physics, Wuhan Institute of Physics and Mathematics, Chinese Academy of Sciences, Wuhan, China*

^g *Laboratory of Inorganic Materials Chemistry (CMI), University of Namur, 61, rue de Bruxelles, B-5000 Namur, Belgium.*

bao-lian.su@fundp.ac.be

xyyang@whut.edu.cn;

baoliansu@whut.edu.cn

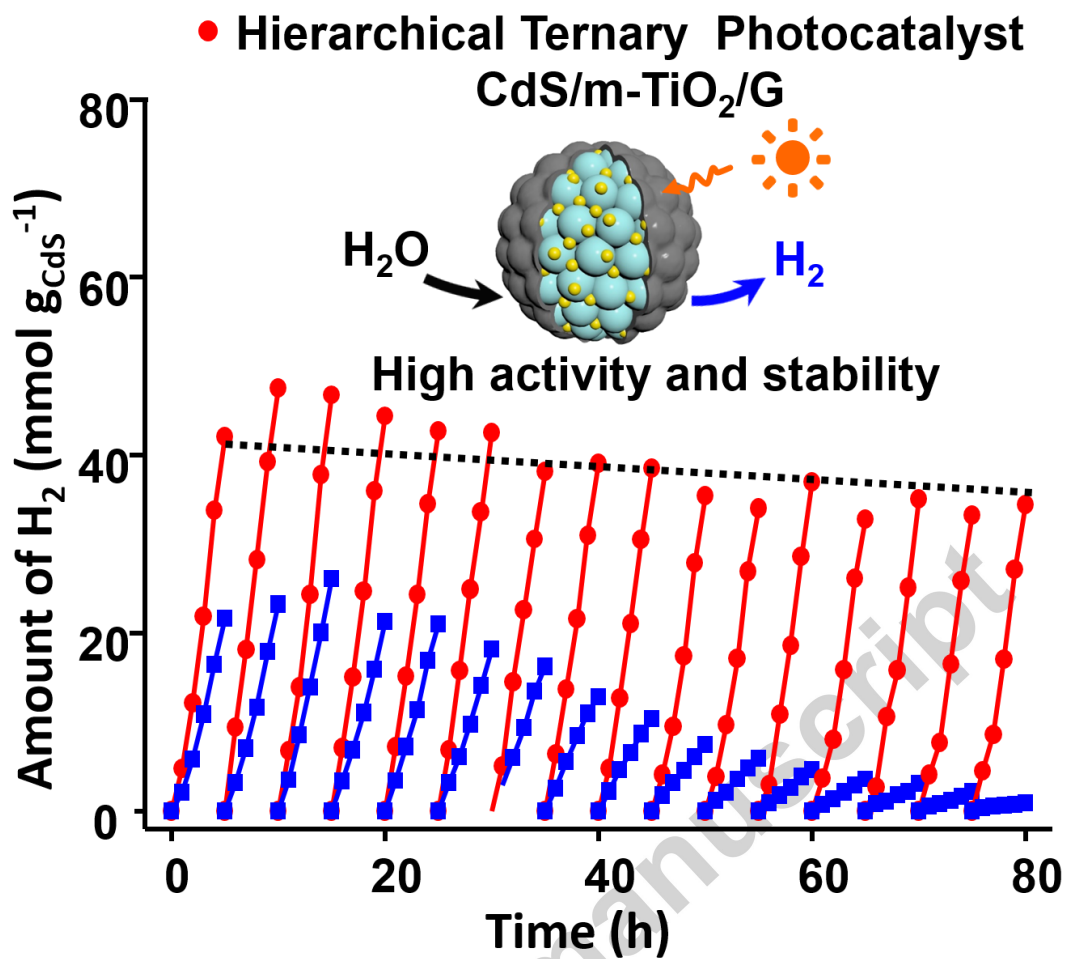
* Corresponding author

Abstract:

Hierarchical semiconductors are the most important photocatalysts, especially for visible light-induced hydrogen production from water splitting. We demonstrate herein a hierarchical electrostatic assembly approach to hierarchical CdS/m-TiO₂/G ternary photocatalyst, which exhibits high photoactivity and excellent photostability (more than twice the activity of pure CdS while 82% of initial photoactivity remained after 15 recycles during 80 hrs irradiation). The ternary nanojunction effect of the photocatalyst has been investigated from orbitals hybrid, bonding energy to atom-stress distortion and nano-interface fusion. And a coherent separation mechanism of charge carriers in the ternary system has been proposed at an atomic/nano scale. This work offers a promising way to inhibit the photocorrosion of CdS and, more importantly, provide new insights for the design of ternary nanostructured photocatalysts with an ideal heterojunction.

Graphical abstract :

A new insight into constructing a hierarchical ternary composite photocatalyst for visible light-induced hydrogen production from water splitting with high activity and stability by electric-triple-layer hierarchical assembly approach. The atomic-scaled heterojunctions of CdS/m-TiO₂/G are beneficial for efficient transformation of photogenerated carriers from the semiconductor, which thus significantly enhance the CdS photoactivity and inhibited the CdS photocorrosion.



Keywords: CdS; mesoporous TiO_2 ; graphene sheets; ternary photocatalysis; visible light-induced water splitting

1. Introduction

Cadmium sulfide (CdS) is considered as one of the most important semiconductors as a visible-light-driven photocatalyst [1-3]. However, it remains a great challenge to protect CdS quantum dots (QDs) from photocorrosion and nano-aggregation, which greatly limits the practical applications of CdS for solar fuel production [4]. There are many successful approaches to enhance the stability of CdS via binary composition techniques including nano-loading [5, 6], nano-coating [7-9], nano-entrapping [10-13] and nano-junctions [14-18]. For example, CdS loaded onto graphene sheets shows high photocatalytic activity [5] and photostability [6] attributed to the strong interaction between CdS and graphene. CdS coated by nanocarbon [3, 7], and conductive polymers [8, 9] can significantly inhibit the photocorrosion due to the confinement effect. While CdS entrapped in open frameworks such as ordered mesostructures [10-12] has also shown to be beneficial for preventing CdS from photocorrosion and aggregation because of the confined space and high dispersity; Nano-junctions such as CdS/TiO₂ [14, 15, 19, 20], CdS/Au [21], CdS/ZnO [16], hexagonal CdS/cubic CdS [17, 18] are often used to promote the photoactivity and photostability of CdS because of the efficient separation of the photogenerated carriers. Notably, it is still not easy to obtain a long-term stable CdS photocatalyst although various protection mechanisms have been discovered. Subsequently, ternary composition techniques are studied, because they might combine the successes of the binary composite [22]. A nice attempt of ternary composites is the entrapment of CdS nanocrystals within macropores of the TiO₂

array, and on-top graphene oxide sheets to cover the TiO₂ array surfaces as an inhibitor of photocorrosion [23, 24]. However, the photoactivity didn't improve drastically due to the relatively low long-range electronic conduction of the TiO₂ arrays. One of the techniques to improve the photoactivity of CdS is by using nanosized composites in order to accelerate the electron-hole separation such as in the hexagonal CdS/Pt/cubic CdS [18] and CdS/TiO₂/Au [25, 26] ternary system. However, due to the incapability of hole inhibition, this structure results in a relatively low photostability of CdS. Further development of a ternary composite is done by using binary CdS nanocomposites within nanoporous structures such as CdS-polyoxo-Ti cluster-MOF, which greatly enhances the photoactivity of CdS, but results in a low chemical and thermal stability of the organic-inorganic hybrids [27]. Ideally, ternary nanocomposite photocatalysts need the various components to integrate together at an atomic or nanosize scale to form ternary nanojunctions that could result in highly efficient electron-hole pair separation [28]. More importantly, the final nanostructure should be highly stable and capable of hole inhibition. It is therefore highly preferred to strive for high structural stability and successful atomic/nanoscale integration of the three components in a ternary composite system, which not only will greatly enhance the stability of nanocomposites, but also greatly improve the activity of CdS.

Recently, core-shell structures have received a lot of attention because these nanostructures can combine functionalities of the various components at a nanoscale and enhance the confined-space catalysis effect, as well as stabilize the nanocatalysts. The composite and nanostructure properties can be integrated into one solid, such as

nanocatalysts and biocatalysts within a hierarchical structure [29-32]. Here we present a hierarchical electrostatic assembly approach to hierarchical CdS/mesoporous TiO₂/graphene (CdS/m-TiO₂/G) as a core-shell ternary visible-light photocatalyst. Very interestingly, the hierarchical CdS/m-TiO₂/G shows a highly increased activity and stability during visible-light-induced photocatalytic H₂ production compared to pure CdS. Furthermore, the ternary nanojunction effect of the hierarchical CdS/m-TiO₂/G has been investigated from orbitals hybrid, bonding energy to atom-stress distortion and nano-interface fusion. And a coherent separation mechanism of charge carriers in the ternary system has been proposed at an atomic/nano scale.

2. Experimental section

2.1 Materials

Hexadecylamine (HDA, 90%, Sigma-Aldrich), Titanium (IV) isopropoxide (TIP, 95%), dimethyl sulfoxide (99.8%), citric acid (99.5%) and Cadmium acetate dehydrate (99.99%) were purchased from Aladdin Industrial Co., China. Other chemical reagents were of analytical grade and were supplied by Sinopharm Chemical Reagent Co., Ltd., China. GO was synthesized by the modified Hummers method [33, 34].

2.2 Preparation of *m*-TiO₂, CdS, CdS/*m*-TiO₂, CdS/*m*-TiO₂/G, CdS/G and TiO₂/G

Pure *m*-TiO₂ were synthesized according to a previous report [35]. To obtain ternary core-shell structured photocatalyst, 0.15 g *m*-TiO₂ was dispersed in 80 mL

DMSO with ultrasonification, then 0.106 g $\text{Cd}(\text{CH}_3\text{COO})_2 \cdot 2\text{H}_2\text{O}$ was added into the dispersion and stirring for 2h (the final weight ratio of CdS is about 20.1%). Followed by adding 3 mL GO solution (2 mg/mL) with continuous stir, the resulting mixture was autoclaved in a Teflon-lined stainless steel vessel at 180 °C for 12 h. The dark yellow solid samples were filtered with acetone and ethanol to remove reactants. To remove free CdS, the final samples were dispersed in water and sonicated for a short time, then collected by centrifugation and dried in air at 60 °C, the obtained sample was labeled as CdS/m-TiO₂/G. For comparison, 0.027, 0.053, 0.213, 0.318 and 0.954 g of $\text{Cd}(\text{CH}_3\text{COO})_2 \cdot 2\text{H}_2\text{O}$ were used for synthesize CdS/m-TiO₂/G, with the final weight ratio of CdS are about 5.2%, 10.2%, 38.6%, 66.3% and 79.3%, respectively. The samples were marked as CdS/m-TiO₂/G-x, x= weight ratio of CdS. CdS/m-TiO₂, CdS/G and m-TiO₂/G nanoparticles were synthesized by the same procedure in the absence of GO, m-TiO₂ and $\text{Cd}(\text{CH}_3\text{COO})_2 \cdot 2\text{H}_2\text{O}$, respectively. CdS was synthesized by the same procedure in the absence of GO and m-TiO₂.

2.3 Characterization

The samples morphology observation was performed on a field emission scanning electron microscope (FESEM, S-4800, HITACHI) and a transmission electron microscope (TEM, JEOL-2100F). The high angle annular dark field (HAADF) and energy-dispersive X-ray spectroscopy (EDS) elemental mapping images were performed on an EDAX Genesis. The power X-ray diffraction (XRD) patterns were recorded on an X-ray diffractometer with Cu K α radiation (D8 Advance, Bruker, $\lambda = 1.5418 \text{ \AA}$). Zeta potentials were measured by Zetasizer Nano Series (ZEN

3600, Malvern). The Brunauer-Emmett-Teller (BET) measurements specific surface area was measured by using a Micromeritics ASAP 3020 system. The pore size distribution for each sample was calculated from the adsorption isotherm branch using the BJH method. The total pore volume was obtained from the amount adsorbed at $P/P_0 = 0.99$. ICP measurements were examined on inductively coupled plasma-atomic emission spectroscopy (ICP-AES, Prodigy7). Fourier transform infrared spectroscopy (FT-IR) spectra were obtained using a Bruker VerTex 80v spectrometer. UV-visible spectra were measured on a UV-visible spectrophotometer (UV-2550, Shimadzu, Japan). X-ray photoelectron spectroscopy (XPS) measurements were performed on a PHI Quantera II, (ULVAC-PHI, Japan) for chemical composition analysis, all binding energies were calibrated to the C1s peak at 284.6 eV. The photoluminescence spectra (PL) were recorded on LS 55 (PERKIN-ELMER) with an excitation wavelength of 300 nm. Time-resolved fluorescence emission spectra were recorded at room temperature with a fluoromax-4 spectrofluorometer (HORIBA Scientific).

2.4 Photocatalytic reactions

Photocatalytic H₂ production was performed in a closed circulation system using a PLS-SXE-300C lamp (Beijing perfectlight Technology Co., Ltd.) with a visible light intensity of *ca.* 158 mW cm⁻² ($\lambda \geq 420$ nm). The lamp was 10 cm away from the reaction solution. 20 mg of CdS or CdS/m-TiO₂/G was suspended in 80 ml of an aqueous solution containing Na₂SO₃ (0.1 M) and Na₂S (0.1 M). The mixture was sealed in a quartz vessel and vacuumed for 10 min to remove the dissolved oxygen, a

continuous magnetic stirrer and cooling water were applied during the experiment. The produced H₂ was analyzed by an Agilent 7890A gas chromatograph (GC) with a thermal conductivity detector (TCD).

The apparent quantum yields (AQY) was measured and calculated by the following equation using a PLS-SXE-300C Xe lamp with 420 nm band-pass filter (120 mW cm⁻²):

$$\text{AQY} = \frac{\text{Number of evolved H molecules} \times 2}{\text{Number of incident photos}} \times 100\%$$

2.5 Photoelectrochemical Measurements

Photocurrent tests were carried out in a conventional three-electrode system using on a CHI 660D electrochemical workstation (Chenhua Instrument, Shanghai, China) with a Pt foil as the counter electrode and a Ag/AgCl reference electrode at a 0.5 V potential bias under a PLS-SXE-300C lamp. The working electrodes were prepared by dispersing catalysts (5 mg) and Nafion solution (100 μ L, 0.5 wt%) in water/ethanol mixed solvent (1 mL, 1:1 v/v) at least 30 min of sonication to form a homogeneous ink. The working electrode was prepared by drop-casting the above ink (50 μ L) onto FTO glass with an area of 1 cm².

3. Results and discussion

The synthesis process and formation mechanism of CdS/m-TiO₂/G are shown in Fig. 1. Surface charges play an important role in the nanoencapsulation of CdS, which could be estimated by measuring the zeta potentials (Table S1). First, the negatively surface of m-TiO₂ (Fig. 1a) ($\zeta = -14.9$ mV) bead is adsorbed by Cd²⁺ forming

m-TiO₂/Cd²⁺ (Fig. 1b) ($\zeta = -11.4$ mV) electrical bilayer with a bridge positive charge (Cd²⁺). When GO is added into the above mixture, the negatively charged GO sheets are attracted electrostatically to bridge positive charge (Cd²⁺) of the m-TiO₂/Cd²⁺ forming a Negative-Positive-Negative electrical triple layer m-TiO₂/Cd²⁺/GO (Fig. 1c) ($\zeta = -19.8$ mV) [36, 37]. In our proposed model, the positive ion acts as a bridge to assemble the two types of negative ions, resulting in the two precursors with surface negative charges self-assemble together. [38, 39] After the solvothermal process, GO can be converted to chemical converted graphene (G); CdS is generated in the confined space of m-TiO₂ and graphene, and the hierarchical CdS/m-TiO₂/G (Fig. 1d) can be finally obtained. The Negative-Positive-Negative electric-triple-layer (Fig. 1e) will not only avail to the hierarchical assembly of m-TiO₂/Cd²⁺/GO, but is also beneficial to the strong linkage (and/or nanofusion) between CdS, m-TiO₂ and graphene to produce a uniform dispersion of CdS in the mesostructure (Fig. 1f).

The morphology and crystal structure of the CdS/m-TiO₂/G are examined by scanning electron microscopy (SEM) (Fig. 2a), XRD (Fig. 2b), HRTEM (Fig. 2c and Fig. 2h~2j, Fig. S3), HAADF-STEM (Fig. 2d) and the corresponding EDX elemental mapping (Fig. 2e-2g). The CdS/m-TiO₂/G beads show a uniform diameter of about 400 nm and consist of individual nanoparticles (Fig. 2a and Fig. S1e). Compared to the pure m-TiO₂ beads (Fig. S1c), a few layers of graphene are clearly visible on the surface of the CdS/m-TiO₂/G beads, and the CdS/m-TiO₂/G have a rougher surface due to the co-deposition of CdS and graphene onto the TiO₂ nanocrystals. Very interestingly, the images (Fig. 2a and Fig. 2c) show no obvious CdS aggregations on

the outlayer of the CdS/m-TiO₂/G by hierarchically electrostatic assembly, probably attributed a priority of absorption and diffusion of Cd²⁺ ions via relative strong electrostatic attraction, high-surface-area effect and capillary action of mesochannels. To avoid the limitation of SEM and TEM at large-scale observation, only CdS and m-TiO₂ as the control sample shown in Fig. S1d presents that the nanosized CdS trends to form around m-TiO₂ and aggregates together. This result strongly suggests that the Negative-Positive-Negative hierarchically electrostatic assembly can prevent CdS from aggregation as compared to the traditional electronic-bi-layer approach. The XRD patterns in Fig. 2b show both m-TiO₂ and CdS diffraction peaks: anatase TiO₂ (JCPDS no. 21-1272) and cubic CdS (JCPDS no. 80-0019). However, the CdS as well as the m-TiO₂ peaks are broad and diffuse due to the nanosize dimension of the particles. The HRTEM image of CdS/m-TiO₂/G in Fig. 2c shows that m-TiO₂ consists of individual nanocrystals with a diameter of about 15 nm; the lattice fringes of 0.35 nm agree with the anatase titania (101) interplanar spacing while the 0.204 nm fringes correspond to the (220) planes of CdS. Meanwhile, the CdS nanoparticles with a size of around 8-10 nm are embedded in the mesochannels of TiO₂ and the CdS/m-TiO₂ nanocomposites are intimately coated by few-layer of graphene sheets with the thickness of 2~4 nm (Fig. 2c). It is clear to be seen the atomic-scaled fusion interface between the graphene sheets and titania oxides surface (inset of Fig. 2c). These results suggest a good protection of the hierarchical structure and a high electron-mobility from CdS to graphene during photocatalysis[40, 41].

The SEM image (Fig. S1a) shows the pure CdS nanoparticles aggregates together, meaning relatively low stability and activity. After being ultrasonic dispersed in water, the CdS exhibits the size of about 8-15 nm as shown by HRTEM in Fig. S1b. The STEM image clearly shows the mesoporous structure in the CdS/m-TiO₂/G (Fig. 2d); the STEM-EDS elemental mapping in Fig. 2e-g demonstrates that Cd element is uniformly distributed over the whole m-TiO₂ single bead, implying the good loading and highly dispersion of CdS into the m-TiO₂ bead. Owing to the electric-triple-layer synthesis process, interfaces of m-TiO₂, CdS and domain boundaries related to the crystal fusion are formed. Interestingly, a different type of crystal fusion domain is formed at the phase edge; it shows a disordered atomic arrangement and strong lattice distortions (pink areas in Fig. 2h, the original HRTEM image is shown in Fig. S3a), which results in a change of lattice periodicity and the generation of structural defects. This unique fusion structure improves the photogenerated charge carrier transfer and significantly increases the number of catalytically active sites, due to the very low interface losses during electron transmission. Notably, the nano-domains of amorphous Ti(IV) or semi-crystalline TiO₂ (pale blue in Fig. 2h~2j and Fig. S3b) with irregular morphology are formed due to the relative low calcined temperature and directly bonded to the CdS grains. This amorphous Ti(IV) has a more negative potential and can act as a hole trapping center [42]. The evidence of lattice fusion between CdS and TiO₂ with anatase and/or amorphous phases is observed in the inverse FFT images of the regions I and II (Fig. 2h~2j). Disordered densely-packed domains are present at the interface between CdS

and anatase TiO₂ (region I, Fig. 2i), due to the lattice stress [43] and strong interface interaction during the solvothermal synthesis. Most importantly, such a mixed-phase structure between CdS and TiO₂ renders a minimum degradation of the carrier mobility. The lattice irregularity around CdS is attributed to the amorphous or semi-crystalline phases of TiO₂ (Fig. 2j and Fig. S3b). These nano-fusion domains caused by heterojunctions of CdS and TiO₂ not only facilitate the separation of carriers, but also can bond the different nanoparticles and enhance the stability of the nanostructure [44].

We further studied the pore size distribution of m-TiO₂, CdS/m-TiO₂ and CdS/m-TiO₂/G by nitrogen sorption measurements. In Fig. S4, both samples exhibit typical IV-type isotherms, indicating the existence of well-developed mesopores. The CdS/m-TiO₂/G sample has a specific surface area of 85.3 m² g⁻¹, an average pore size of 13.3 nm and a pore volume of 0.23 cm³ g⁻¹. Compared to m-TiO₂ (Table S2), the slight decrease of CdS/m-TiO₂/G not only indicates the successful loading of CdS and the coating of graphene, but also prevents CdS from aggregation to block the mesopores. Meanwhile, the CdS/m-TiO₂ sample has obviously decreased its specific surface area, average pore size and pore volume, due to the aggregation of CdS in the mesostructure in absence of the graphene sheets, which is in good agreement with the TEM and SEM data.

The photocatalytic H₂ production and inhibition of the photocorrosion of CdS in practical application over m-TiO₂, CdS, m-TiO₂/G, CdS/m-TiO₂, CdS/G and CdS/m-TiO₂/G is examined by using a mixed Na₂S and Na₂SO₃ aqueous solution

under visible light irradiation. The comparison of the H₂ production of CdS/m-TiO₂/G samples (with the final weight ratio of CdS are 5.2%, 10.2%, 20.1%, 38.6%, 66.3% and 79.3% from the ICP results) are shown in Fig. S5a. With the increasing of the content of the CdS, the photoactivity of the CdS/m-TiO₂/G decrease, which is due to highly disperse of CdS at relatively lower level of the content. The CdS/m-TiO₂/G-5.2%, CdS/m-TiO₂/G-10.2% and CdS/m-TiO₂/G-20.1% show higher H₂ production rate in comparison of CdS/m-TiO₂/G-38.6%, CdS/m-TiO₂/G-66.3%, CdS/m-TiO₂/G-79.3%. Notably, the CdS/m-TiO₂/G-38.6% shows aggregation of the nanosized CdS (Fig. S5b), suggesting the overloading of CdS in the system of CdS/m-TiO₂/G. The 20.1% of weight ratio of CdS is chosen (short for CdS/m-TiO₂/G), which is far more than the amount of sensitizing treatment and presents high photoactivity and high dispersion. In Fig. S6, ternary CdS/m-TiO₂/G shows the highest H₂ production activity up to 8.4 mmol (h g_{CdS})⁻¹, with an AQY of *ca.* 9% at 420 nm monochromatic light irradiation. The high photoactivity is directly attributed to the high dispersion of CdS and the ternary nano-junction with CdS/m-TiO₂/G, which greatly improve the separation of photogenerated electrons and holes [5, 45]. Note that there is no H₂ generated without the CdS component, suggesting that samples without CdS are likely not active under visible light irradiation. Besides, binary CdS/m-TiO₂ and CdS/G also display a higher photoactivity than pure CdS, which means that the introduction of m-TiO₂ and graphene sheets is beneficial for the photocatalytic activity. More importantly, CdS/m-TiO₂/G shows a very high photostability in comparison with pure CdS (Fig. 3).

For example, after one recycle, the CdS/m-TiO₂/G shows a very high H₂ production activity up to 9.5 mmol (h g_{CdS})⁻¹; this is about 2.1 times more than pure CdS. Even after 40 hrs (7 recycles) and 60 hrs (11 recycles), CdS/m-TiO₂/G remained at 92.9% and 87.9% of the initial photoactivity. In contrast, the photoactivity of pure CdS sees a significant decrease and only keeps 59.4% and 21.2% activity, respectively. After 80 hrs (15 recycles) irradiation, the photostability of CdS/m-TiO₂/G is observably higher (82% of the initial photoactivity remain) than the photostability of CdS, CdS/G, and CdS/m-TiO₂ (Fig. S7) and all the CdS, CdS/G, CdS/m-TiO₂ show very lack of photostability (about 4%, 25% and 35% of the initial photoactivity). It is therefore believed to the very low content of impurities (CdS, CdS/G, CdS/m-TiO₂) in our ternary CdS/m-TiO₂/G photocatalyst. As a result, we not only enhanced the unit photoactivity of CdS but also highly improved its long-term photostability, which mainly attributed to the unique ternary composition at the atomic/nano scale and proposed two electron transfer paths: the photogenerated electrons can be injected from CdS to m-TiO₂ and to graphene [24] or it can be injected from CdS to graphene directly [5]. Moreover, the HRTEM image (inset of Fig. 3) shows the ternary composition nanostructure of CdS/m-TiO₂/G to be almost unchanged after 80 hrs of photocatalytic reaction. Also the corresponding XRD patterns reveal a stable crystal structure (Fig. S8). The CdS nanoparticles, between the TiO₂ and the graphene, still show a good crystallinity and a spherical shape with a size of 8-10 nm (Fig. 3), illustrating that CdS can maintain its activity and nanostructure during long-term photocatalysis. Moreover, the coherent mesostructure of the CdS, TiO₂ and graphene

is kept. Thanks to the nano-encapsulated core-shell structure and ternary composition at an atomic/nano scale, the encapsulated CdS nanoparticles that *in situ* uniformly generated within m-TiO₂ and confined by outer-layered graphene, are not only preventing agglomeration, but also avoid the exposure and photocorrosion of CdS.

To further confirm the ternary nanojunction and the synergetic effect of CdS/m-TiO₂/G on the photostability, the interface interaction and chemistry of the samples CdS/m-TiO₂/G, m-TiO₂ and CdS are studied by FT-IR and UV-vis diffuse reflection analysis (Fig. S9). The peaks at 1625.9 cm⁻¹ of all the samples are ascribed to the surface -OH groups probably caused by chemical synthesis of the nanomaterials; the broad peaks at 728.7 cm⁻¹ (m-TiO₂ and CdS/m-TiO₂/G) are assigned to the Ti-O-Ti stretching and bending vibrational modes [46]. The peak at 1109 cm⁻¹ and 620 cm⁻¹ of CdS could be attributed to the S=O bond of the CdS complex [47] and Cd-S symmetric stretching from CdS [48]. The CdS/m-TiO₂/G shows clearly weakened intensity of the S=O and Cd-S peaks, while there is a new weak peak at 629 cm⁻¹ ascribed to the Ti-O-C bond [49, 50], indicating the formation of a new chemical bond between the graphene sheets and TiO₂ (Fig. S9a). A comparison of the UV-vis diffuse reflection spectra of samples m-TiO₂, CdS and CdS/m-TiO₂/G is displayed in Fig. S9b. The absorption edge of CdS/m-TiO₂/G is red-shifted in comparison with pure CdS, implying that the coating of graphene influences the energy band gap of CdS (shown in the inset). The enhanced light absorption relates to the formation of Ti-C bonds between TiO₂ and graphene [51].

Thus, the graphene sheets are firmly coated and possibly bond onto the surface of m-TiO₂, improving the absorption efficiency of light.

The chemical state for CdS, m-TiO₂, CdS/m-TiO₂ and CdS/m-TiO₂/G is deduced from the XPS analysis. Fig. 4a shows the C 1s, Ti 2p and Cd 3d high resolution of CdS/m-TiO₂/G. The binding energy of 284.6 eV is attributed to the C-C, C=C and C-H bonds. Oxygen-containing groups such as the C-O bond (286.2 eV), C=O bond (287.1 eV) and O-C=O (288.7 eV) show very low intensities and indicate the almost full reduction of GO. The peak located at 282.6 eV is assigned to the presence of a Ti-C bond [52-54], which is caused by the binding of graphene and TiO₂. The spectrum of Ti 2p shows two spin-orbit peaks Ti 2p_{3/2} and Ti 2p_{1/2} with a bonding energy of 458.7 and 464.5 eV, representing the normal Ti⁴⁺ valence state in TiO₂. The two peak deconvolutions in the binding energies of 457.5 and 463.3 eV suggest the presence of Ti³⁺ in addition to Ti⁴⁺ chemical state [55, 56], and the two other peaks centered at 465.8 and 460.2 eV are attributed to the Ti-C bond [56-59], which is in accordance with C 1s results. In addition, the formation of the Ti-O-C bond was also confirmed by the XPS spectra of O 1s (Fig. S10a). The main peak centered at 530.1 eV correspond to Ti-O-Ti (lattice O). The peak with lower binding energy located at 528.9 eV is attributed to Ti³⁺-O [60]. More over, the peak deconvolution at 531 eV correspond to Ti-O-C bond [60] which has also been observed in FT-IR spectrum. Models of the new chemical bonds, generated at the interface of binary and ternary systems between CdS, TiO₂ and graphene, are proposed in Fig. 4bi~4biii. For CdS/m-TiO₂, when CdS combines with TiO₂, the surface Ti-O-Ti bonds in TiO₂ are

broken, Cd will bond with lattice oxygen to form a Cd-O-Ti bond. This leads to a decrease of the electron-electron repulsion around the Cd atoms and facilitates the Cd core level moving toward higher bonding energy (Fig. 4c, Fig. S10) [61, 62]. The other electron hybrids such as Cd-O-Ti and Ti-S-Cd bonds in CdS/m-TiO₂ (Fig. 4b i), and a Cd-C bond in CdS/G (Fig. 4bii) could also be estimated by Cd 3d core level shift (Fig. 4c). As to visible light excitation, the directions of the photogenerated electron transfer will depend on the relative position of the CB and VB of the semiconductors (from CdS to TiO₂ and/or graphene). Compared to the binary systems, the ternary CdS/m-TiO₂/G with atomic and nanoscale composition, the bonding varieties enhance the bonding energy and provide various paths for the electron transmission from Cd to the TiO₂ and graphene (Fig. 4biii). More direct evidence is provided by the Cd 3d chemical shift (Fig. 4c). In the case of CdS/m-TiO₂, CdS/G and CdS/m-TiO₂/G, the XPS peaks for Cd 3d_{5/2} have a chemical shift of 0.2 eV, 0.3 eV and 0.4 eV respectively, compared to that of CdS, (Fig. 4b and Fig. S10c). Compared to the binary systems, the increment of the Cd 3d core level shift in the ternary system confirms that the ternary composites at atomic/nano scale enhance the bonding energy, resulting in a structural and/or bonding stability and electron-transmission varieties. On the other hand, the efficient transfer of charge carriers across the semiconductor interface is the key for photocatalytic efficiency, and the heterostructure is beneficial to the interfacial charge transfer [63-65]. Therefore, the ternary CdS/m-TiO₂/G, not only involves the Cd-O-Ti, Ti-C, Cd-S-Ti and Cd-C bonds varieties, but also has a more stabilized chemical environment due to the coating of graphene and a broader

tendency of the electron cloud to move towards graphene. Thus results in photogenerated electron transfer to graphene in a multiway. The transient photocurrent responses are shown in Fig. 4d, as expected, further confirm that CdS/m-TiO₂/G shows the highest photocurrent intensity compared to CdS, CdS/G and CdS/m-TiO₂ due to the dual electron transfer pathways in the ternary system. Moreover, the electron transfer among CdS, TiO₂ and graphene in both binary and ternary composite photocatalysts is investigated by photoluminescence (PL) (Fig. S11). The PL intensity of CdS in both the binary and ternary system has decreased, this emission peak is assigned to a recombination from the excitonic state. The dramatic decrease of the PL signals of CdS/m-TiO₂/G indicates a significant separation of photogenerated carriers due to the highly efficient electron transfer from the CdS to the TiO₂ and graphene. To further understand charge carrier dynamics, time-resolved photoluminescence decays are introduced to evaluate the structures and charge transfer between CdS/m-TiO₂/G and counterparts. Since the long lifetime of photogenerated holes and electrons, the efficient charge separation will show a slow PL signal decay [66]. As presented in Fig. S12 and Table S4, fast (4.09~4.47 ns) and slow (21.9~23.8 ns) lifetime components are observed. Nanosized CdS shows the shortest decay time due to the low charge separation efficiency. Binary CdS/G and CdS/m-TiO₂ exhibit a faster PL decay compared to ternary CdS/m-TiO₂/G, suggesting difference between the binary and ternary model. The two ways of electron transfer are therefore proposed to better understand the possibility of

separation of photogenerated carriers of ternary CdS/m-TiO₂/G through interface charge transfer.

When the photocatalytic reaction occurs, photogenerated electrons from the valence band (VB) of CdS move to its conduction band (CB), leaving photogenerated holes in the VB. Subsequently, photogenerated electrons are transferred at the CdS/m-TiO₂, m-TiO₂/G and CdS/G interface due to their matching CB position and intimate interfacial contact by two electron transfer paths: the photogenerated electrons can be injected from CdS to m-TiO₂ and to graphene or it can be injected from CdS to graphene directly. Therefore, photogenerated electrons are both driven to the graphene layer and make the graphene layer the active site for adsorption of H⁺ and promote surface chemical reactions for H₂ production. Besides, CdS directly bonds to amorphous Ti(IV) domains, which thus facilitates the photogenerated holes to migrate from CdS to the amorphous Ti(IV). The amorphous Ti(IV) domains have a more negative potential and act as efficient hole capture centers [42, 67, 68]. Thus, the photoactivity of the sample is enhanced due to the improved separation efficiency of the photogenerated electron-hole pairs. On the other hand, photogenerated holes are trapped in amorphous Ti(IV) and rapidly consumed by the sacrificial reagent instead of oxidizing CdS. Meanwhile, nanofusion domains of CdS/m-TiO₂/G act as interfacial bonding, for structure-stability and photostability. Therefore, the advantageous combination of visible light harvesting induced by the core-shell structure and the ternary composition system constructed by the lattice binding among three components are responsible for the stable and excellent photocatalytic H₂ evolution.

4. Conclusions

In summary, a CdS/m-TiO₂/G ternary composite photocatalyst has been successfully prepared via Negative-Positive-Negative hierarchical electrostatic assembly synthesis and exhibits an extremely high H₂ production rate and long-term photostability. This superior performance is attributed to three reasons. Firstly, the m-TiO₂/Cd²⁺/GO electric tri-layer is beneficial to interfacial nanofusion of CdS/m-TiO₂/G and a high dispersion of CdS in a core-shell structure, resulting in a high structural stability and less leaching of CdS. Secondly, the atomic-scaled heterojunctions in CdS/m-TiO₂/G are beneficial for multiple and efficient transfer of photogenerated carriers from the semiconductor, which thus significantly enhances the CdS photoactivity. Thirdly, the photogenerated holes are rapidly transferred to the amorphous Ti(IV) domains, booting their oxidation reaction and enhancing the photostability. This work offers a promising way to inhibit the photocorrosion of CdS and, more importantly, provides a new insight for the design of ternary nanostructured photocatalysts with optimized heterojunctions.

Acknowledgements

This work supported by National Key R&D Program of China (2017YFC1103800), Program for Changjiang Scholars and Innovative Research Team in University (IRT_15R52), National Natural Science Foundation of China (U1663225, U1662134, 51472190, 51611530672, 21711530705, 51503166, 51602236, 21706199), International Science & Technology Cooperation Program of China (2015DFE52870), Natural Science Foundation of Hubei Province (2016CFA033, 2017CFB487), Open

Project Program of State Key Laboratory of Petroleum Pollution Control (PPC2016007) CNPC Research Institute of Safety and Environmental Technology., China Postdoctoral Science Foundation (2016M592400), Fundamental Research Funds for the Central Universities (WUT: 2017IVB012).

Appendix A. Supporting information

Supplementary data associated with this article can be found in the online version at <http://dx.doi.org/10.1016/j.nanoen. xxxx. xx. xxx>.

References

- [1] L. Shang, B. Tong, H. Yu, G. I. N. Waterhouse, C. Zhou, Y. Zhao, M. Tahir, L.-Z. Wu, C.-H. Tung, T. Zhang, CdS nanoparticle-decorated cd nanosheets for efficient visible light-driven photocatalytic hydrogen evolution, *Adv. Energy Mater.* 6 (2016) DOI: 10.1002/aenm.201501241.
- [2] J. Kou, C. Lu, J. Wang, Y. Chen, Z. Xu, R. S. Varma, Selectivity enhancement in heterogeneous photocatalytic transformations, *Chem. Rev.* 117 (2017) 1445-1514.
- [3] Q. Li, X. Li, S. Wageh, A. Al - Ghamdi, J. Yu, CdS/Graphene nanocomposite photocatalysts, *Adv. Energy Mater.* 5 (2015) DOI: 10.1002/aenm.201500010.

- [4] K. Deng, L. Li, CdS Nanoscale photodetectors, *Adv. Mater.* 26 (2014) 2619-2635.
- [5] Q. Li, B. Guo, J. Yu, J. Ran, B. Zhang, H. Yan, J. R. Gong, Highly efficient visible-light-driven photocatalytic hydrogen production of CdS-cluster-decorated graphene nanosheets, *J. Am. Chem. Soc.* 133 (2011) 10878-10884.
- [6] P. Zeng, Q. Zhang, T. Peng, X. Zhang, One-pot synthesis of reduced graphene oxide-cadmium sulfide nanocomposite and its photocatalytic hydrogen production, *Phys. Chem. Chem. Phys.* 13 (2011) 21496-21502.
- [7] Y. Hu, X. Gao, L. Yu, Y. Wang, J. Ning, S. Xu, X. W. Lou, Carbon-coated CdS petalous nanostructures with enhanced photostability and photocatalytic Activity, *Angew. Chem. Int. Ed.* 52 (2013) 5636-5639.
- [8] H. Zhang, Y. Zhu, Significant visible photoactivity and antiphotocorrosion performance of CdS photocatalysts after monolayer polyaniline hybridization, *J. Phys. Chem. C* 114 (2010) 5822-5826.
- [9] C. Wang, L. Wang, J. Jin, J. Liu, Y. Li, M. Wu, L. Chen, B. Wang, X. Yang, B.-L. Su, Probing effective photocorrosion inhibition and highly improved photocatalytic hydrogen production on monodisperse PANI@CdS core-shell nanospheres, *Appl. Catal., B: Environ.* 188 (2016) 351-359.
- [10] G. Guan, T. Kida, K. Kusakabe, K. Kimura, X. Fang, T. Ma, E. Abe, A. Yoshida, Photocatalytic H₂ evolution under visible light irradiation on CdS/ETS-4 composite, *Chem. Phys. Lett.* 385 (2004) 319-322.

- [11]G. Guan, T. Kida, K. Kusakabe, K. Kimura, E. Abe, A. Yoshida, Photocatalytic activity of CdS nanoparticles incorporated in titanium silicate molecular sieves of ETS-4 and ETS-10, *Appl. Catal. A- Gen.* 295 (2005) 71-78.
- [12]R. Peng, D. Zhao, J. Baltrusaitis, C.-M. Wu, R. T. Koodali, Visible light driven photocatalytic evolution of hydrogen from water over CdS encapsulated MCM-48 materials, *RSC Advances* 2 (2012) 5754-5767.
- [13]S. Y. Ryu, W. Balcerski, T. K. Lee, M. R. Hoffmann, Photocatalytic production of hydrogen from water with visible light using hybrid catalysts of CdS attached to microporous and mesoporous silicas, *J. Phys. Chem. C* 111 (2007) 18195-18203.
- [14]Y. Tak, H. Kim, D. Lee, K. Yong, Type-II CdS nanoparticle-ZnO nanowire heterostructure arrays fabricated by a solution process: enhanced photocatalytic activity, *Chem. Commun.* (2008) 4585-4587.
- [15]H. Yan, J. Yang, G. Ma, G. Wu, X. Zong, Z. Lei, J. Shi, C. Li, Visible-light-driven hydrogen production with extremely high quantum efficiency on Pt-PdS/CdS photocatalyst, *J. Catal.* 266 (2009) 165-168.
- [16]H. Zhao, Y. Dong, P. Jiang, G. Wang, H. Miao, R. Wu, L. Kong, J. Zhang, C. Zhang, Light-assisted preparation of a ZnO/CdS nanocomposite for enhanced photocatalytic H_2 evolution: an insight into importance of in situ generated ZnS, *ACS Sustain. Chem. Eng.* 3 (2015) 969-977.
- [17]K. Li, M. Han, R. Chen, S.-L. Li, S.-L. Xie, C. Mao, X. Bu, X.-L. Cao, L.-Z. Dong, P. Feng, Y.-Q. Lan, Hexagonal@cubic CdS core@shell nanorod photocatalyst

for highly active production of H₂ with unprecedented stability, *Adv. Mater.* 28 (2016) 8906-8911.

[18] L. A. Silva, S. Y. Ryu, J. Choi, W. Choi, M. R. Hoffmann, Photocatalytic hydrogen production with visible light over Pt-interlinked hybrid composites of cubic-phase and hexagonal-phase CdS, *J. Phys. Chem. C* 112 (2008) 12069-12073.

[19] H. Park, W. Choi, M. R. Hoffmann, Effects of the preparation method of the ternary CdS/TiO₂/Pt hybrid photocatalysts on visible light-induced hydrogen production, *J. Mater. Chem.* 18 (2008) 2379-2385.

[20] J. Zhang, Z. Zhu, Y. Tang, K. Müllen, X. Feng, Titania nanosheet-mediated construction of a two-dimensional titania/cadmium sulfide heterostructure for high hydrogen evolution activity, *Adv. Mater.* 26 (2014) 734-738.

[21] Q. Zhao, M. Ji, H. Qian, B. Dai, L. Weng, J. Gui, J. Zhang, M. Ouyang, H. Zhu, Controlling structural symmetry of a hybrid nanostructure and its effect on efficient photocatalytic hydrogen evolution, *Adv. Mater.* 26 (2014) 1387-1392.

[22] M. Chen, J. Gu, C. Sun, Y. Zhao, R. Zhang, X. You, Q. Liu, W. Zhang, Y. Su, H. Su, D. Zhang, Light-driven overall water splitting enabled by a photo-dember effect realized on 3d plasmonic structures, *ACS Nano* 10 (2016) 6693-6701.

[23] Y. Tang, X. Hu, C. Liu, Perfect inhibition of CdS photocorrosion by graphene sheltering engineering on TiO₂ nanotube array for highly stable photocatalytic activity, *Phys. Chem. Chem. Phys.* 16 (2014) 25321-25329.

- [24]J. Xian, D. Li, J. Chen, X. Li, M. He, Y. Shao, L. Yu, J. Fang, TiO₂ nanotube array · graphene · CdS quantum dots composite film in z-scheme with enhanced photoactivity and photostability, *ACS Appl. Mater. Inter.* 6 (2014) 13157-13166.
- [25]H. Zhou, L. Ding, T. X. Fan, J. Ding, D. Zhang, Q. X. Guo, Leaf-inspired hierarchical porous CdS/Au/N-TiO₂ heterostructures for visible light photocatalytic hydrogen evolution, *Appl. Catal. B-Environ.* 147 (2014) 221-228.
- [26]J. Fang, L. Xu, Z. Zhang, Y. Yuan, S. Cao, Z. Wang, L. Yin, Y. Liao, C. Xue, Au@TiO₂-CdS ternary nanostructures for efficient visible-light-driven hydrogen generation, *ACS Appl. Mater. Inter.* 5 (2013) 8088-8092.
- [27]Z. Jiang, J. Liu, M. Gao, X. Fan, L. Zhang, J. Zhang, Assembling polyoxo-titanium clusters and cds nanoparticles to a porous matrix for efficient and tunable H₂-evolution activities with visible light, *Adv. Mater.* 29 (2017) DOI: 10.1002/adma.201603369.
- [28]H. Zhou, P. Li, J. Liu, Z. P. Chen, L. Q. Liu, D. Dontsova, R. Y. Yan, T. X. Fan, D. Zhang, J. H. Ye, Biomimetic polymeric semiconductor based hybrid nanosystems for artificial photosynthesis towards solar fuels generation via CO₂ reduction, *Nano Energy* 25 (2016) 128-135.
- [29]J. Ying, Z.-Y. Hu, X.-Y. Yang, H. Wei, Y.-X. Xiao, C. Janiak, S.-C. Mu, G. Tian, M. Pan, G. Van Tendeloo, B.-L. Su, High viscosity to highly dispersed PtPd bimetallic nanocrystals for enhanced catalytic activity and stability, *Chem. Commun.* 52 (2016) 8219-8222.

- [30] J. Ying, X.-Y. Yang, Z.-Y. Hu, S.-C. Mu, C. Janiak, W. Geng, M. Pan, X. Ke, G. Van Tendeloo, B.-L. Su, One particle@one cell: Highly monodispersed PtPd bimetallic nanoparticles for enhanced oxygen reduction reaction, *Nano Energy* 8 (2014) 214-222.
- [31] B. Li, S. Bai, X. Wang, M. Zhong, Q. Yang, C. Li, Hydration of epoxides on [Co(III)(salen)] encapsulated in silica-based nanoreactors, *Angew. Chem. Int. Ed.* 51 (2012) 11517-11521.
- [32] X. Liu, S. Bai, Y. Yang, B. Li, B. Xiao, C. Li, Q. Yang, Enantioselective carbonyl-ene reaction on BINOLate/titanium catalyst encapsulated in magnetic nanoreactors, *Chem. Commun.* 48 (2012) 3191-3193.
- [33] W. S. Hummers Jr, R. E. Offeman, Preparation of graphitic oxide, *J. Am. Chem. Soc.* 80 (1958) 1339-1339.
- [34] N. I. Kovtyukhova, P. J. Ollivier, B. R. Martin, T. E. Mallouk, S. A. Chizhik, E. V. Buzaneva, A. D. Gorchinskiy, Layer-by-layer assembly of ultrathin composite films from micron-sized graphite oxide sheets and polycations, *Chem. Mater.* 11 (1999) 771-778.
- [35] D. Chen, L. Cao, F. Huang, P. Imperia, Y.-B. Cheng, R. A. Caruso, Synthesis of monodisperse mesoporous titania beads with controllable diameter, high surface areas, and variable pore diameters (14-23 nm), *J. Am. Chem. Soc.* 132 (2010) 4438-4444.
- [36] N. Jiang, X.-Y. Yang, G.-L. Ying, L. Shen, J. Liu, W. Geng, L.-J. Dai, S.-Y. Liu, J. Cao, G. Tian, T.-L. Sun, S.-P. Li, B.-L. Su, "Self-repairing" nanoshell for cell protection, *Chem. Sci.* 6 (2015) 486-491.

- [37] N. Jiang, X.-Y. Yang, Z. Deng, L. Wang, Z.-Y. Hu, G. Tian, G.-L. Ying, L. Shen, M.-X. Zhang, B.-L. Su, A stable, reusable, and highly active photosynthetic bioreactor by bio-interfacing an individual cyanobacterium with a mesoporous bilayer nanoshell, *Small* 11 (2015) 2003-2010.
- [38] P. Behrens, Voids in variable chemical surroundings: mesoporous metal oxides. Behrens, P. *Angew. Chem. Int. Ed.* 35 (1996) 515-518.
- [39] Q. Huo, D. I. Margolese, U. Ciesla, D. G. Demuth, P. Feng, T. E. Gier, P. Sieger, A. Firouzi, B. F. Chmelka, Organization of organic molecules with inorganic molecular species into nanocomposite biphasic arrays, *Chem. Mater.* 6 (1994) 1176-1191.
- [40] X. Wang, L. Zhi, K. Müllen, Transparent, conductive graphene electrodes for dye-sensitized solar cells, *Nano Lett.* 8 (2008) 323-327.
- [41] Y. Lu, X.-Y. Yang, B.-L. Su, Self-assembly to monolayer graphene film with high electrical conductivity, *J. Energy Chem.* 22 (2013) 52-57.
- [42] M. Liu, R. Inde, M. Nishikawa, X. Qiu, D. Atarashi, E. Sakai, Y. Nosaka, K. Hashimoto, M. Miyauchi, Enhanced photoactivity with nanocluster-grafted titanium dioxide photocatalysts, *ACS Nano* 8 (2014) 7229-7238.
- [43] L. Bu, N. Zhang, S. Guo, X. Zhang, J. Li, J. Yao, T. Wu, G. Lu, J.-Y. Ma, D. Su, X. Huang, Biaxially strained PtPb/Pt core/shell nanoplate boosts oxygen reduction catalysis, *Science* 354 (2016) 1410-1414.

- [44] X.-Y. Yang, L.-H. Chen, Y. Li, J. C. Rooke, C. Sanchez, B.-L. Su, Hierarchically porous materials: synthesis strategies and structure design, *Chem. Soc. Rev.* 46 (2017) 481-558.
- [45] P. Zhou, J. Yu, M. Jaroniec, All-solid-state z-scheme photocatalytic systems, *Adv. Mater.* 26 (2014) 4920-4935.
- [46] P. Xu, J. Lu, T. Xu, S. Gao, B. Huang, Y. Dai, I₂-hydrosol-seeded growth of (I₂)_n-C-codoped meso/nanoporous TiO₂ for visible light-driven photocatalysis, *J. Phys. Chem. C* 114 (2010) 9510-9517.
- [47] M. E. Wankhede, S. K. Haram, Synthesis and characterization of Cd-DMSO complex capped CdS nanoparticles, *Chem. Mater.* 15 (2003) 1296-1301.
- [48] S. S. Mali, S. K. Desai, D. S. Dalavi, C. A. Betty, P. N. Bhosale, P. S. Patil, CdS-sensitized TiO₂ nanocorals: hydrothermal synthesis, characterization, application, *Photochemical & Photobiological Sciences* 10 (2011) 1652-1658.
- [49] B. Qiu, M. Xing, J. Zhang, Mesoporous TiO₂ Nanocrystals grown in situ on graphene aerogels for high photocatalysis and lithium-ion batteries, *J. Am. Chem. Soc.* 136 (2014) 5852-5855.
- [50] S. Sakthivel, H. Kisch, Daylight Photocatalysis by carbon-modified titanium dioxide, *Angew. Chem. Int. Ed.* 42 (2003) 4908-4911.
- [51] X.-J. Lv, W.-F. Fu, H.-X. Chang, H. Zhang, J.-S. Cheng, G.-J. Zhang, Y. Song, C.-Y. Hu, J.-H. Li, Hydrogen evolution from water using semiconductor nanoparticle/graphene composite photocatalysts without noble metals, *J. Mater. Chem.* 22 (2012) 1539-1546.

- [52] I. Hiroshi, W. Yuka, H. Kazuhito, Carbon-doped anatase TiO₂ powders as a visible-light sensitive photocatalyst, *Chem. Lett.* 32 (2003) 772-773.
- [53] O. Akhavan, E. Ghaderi, Photocatalytic reduction of graphene oxide nanosheets on TiO₂ thin film for photoinactivation of bacteria in solar light irradiation, *J. Phys. Chem. C* 113 (2009) 20214-20220.
- [54] S. Yin, M. Komatsu, Q. Zhang, F. Saito, T. Sato, Synthesis of visible-light responsive nitrogen/carbon doped titania photocatalyst by mechanochemical doping, *Asian J. Mater. Sci.* 42 (2007) 2399-2404.
- [55] L.-C. Chen, Y.-C. Ho, W.-S. Guo, C.-M. Huang, T.-C. Pan, Enhanced visible light-induced photoelectrocatalytic degradation of phenol by carbon nanotube-doped TiO₂ electrodes, *Electrochim. Acta* 54 (2009) 3884-3891.
- [56] O. Akhavan, R. Azimirad, S. Safa, M. M. Larijani, Visible light photo-induced antibacterial activity of CNT-doped TiO₂ thin films with various CNT contents, *J. Mater. Chem.* 20 (2010) 7386-7392.
- [57] Q. Huang, S. Tian, D. Zeng, X. Wang, W. Song, Y. Li, W. Xiao, C. Xie, Enhanced photocatalytic activity of chemically bonded TiO₂/graphene composites based on the effective interfacial charge transfer through the C-Ti Bond, *ACS Catal.* 3 (2013) 1477-1485.
- [58] Y. Yang, P. Gao, Y. Wang, L. Sha, X. Ren, J. Zhang, Y. Chen, T. Wu, P. Yang, X. Li, A direct charge transfer from interface to surface for the highly efficient spatial separation of electrons and holes: The construction of Ti-C bonded interfaces

in TiO₂-C composite as a touchstone for photocatalytic water splitting, *Nano Energy* 33 (2017) 29-36.

[59]Z. Hu, Y. Huang, S. Sun, W. Guan, Y. Yao, P. Tang, C. Li, Visible light driven photodynamic anticancer activity of graphene oxide/TiO₂ hybrid, *Carbon* 50 (2012) 994-1004.

[60]T.-D. Nguyen-Phan, V. H. Pham, E. J. Kim, E.-S. Oh, S. H. Hur, J. S. Chung, B. Lee, E. W. Shin, Reduced graphene oxide-titanate hybrids: Morphologic evolution by alkali-solvothermal treatment and applications in water purification, *Appl. Surf. Sci.* 258 (2012) 4551-4557.

[61]Y.-G. Yu, G. Chen, L.-X. Hao, Y.-S. Zhou, Y. Wang, J. Pei, J.-X. Sun, Z.-H. Han, Doping La into the depletion layer of the Cd_{0.6}Zn_{0.4}S photocatalyst for efficient H₂ evolution, *Chem. Commun.* 49 (2013) 10142-10144.

[62]P. K. Babu, A. Lewera, J. H. Chung, R. Hunger, W. Jaegermann, N. Alonso-Vante, A. Wieckowski, E. Oldfield, Selenium becomes metallic in ru-se fuel cell catalysts: An EC-NMR and XPS investigation, *J. Am. Chem. Soc.* 129 (2007) 15140-15141.

[63]P. V. Kamat, Manipulation of charge transfer across semiconductor interface. A criterion that cannot be ignored in photocatalyst design, *J. Phys. Chem. Lett.* 3 (2012) 663-672.

[64]P. Li, X. Zhao, C.-j. Jia, H. Sun, L. Sun, X. Cheng, L. Liu, W. Fan, ZnWO₄/BiOI heterostructures with highly efficient visible light photocatalytic activity: the case of interface lattice and energy level match, *J. Mater. Chem. A* 1 (2013) 3421-3429.

- [65]Z. Lu, L. Zeng, W. Song, Z. Qin, D. Zeng, C. Xie, In situ synthesis of C-TiO₂/g-C₃N₄ heterojunction nanocomposite as highly visible light active photocatalyst originated from effective interfacial charge transfer, *Appl. Catal., B: Environ.* 202 (2017) 489-499.
- [66]L. Liu, Z. Ji, W. Zou, X. Gu, Y. Deng, F. Gao, C. Tang, L. Dong, In situ loading transition metal oxide clusters on TiO₂ nanosheets as co-catalysts for exceptional high photoactivity, *ACS Catal.* 3 (2013) 2052-2061.
- [67]N. O. Gopal, H.-H. Lo, S.-C. Sheu, S.-C. Ke, A potential site for trapping photogenerated holes on rutile TiO₂ surface as revealed by EPR spectroscopy: An avenue for enhancing photocatalytic activity, *J. Am. Chem. Soc.* 132 (2010) 10982-10983.
- [68]H. Yu, X. Huang, P. Wang, J. Yu, Enhanced photoinduced-stability and photocatalytic activity of CdS by dual amorphous cocatalysts: Synergistic effect of Ti(IV)-hole cocatalyst and Ni(II)-electron cocatalyst, *J. Phys. Chem. C* 120 (2016) 3722-3730.

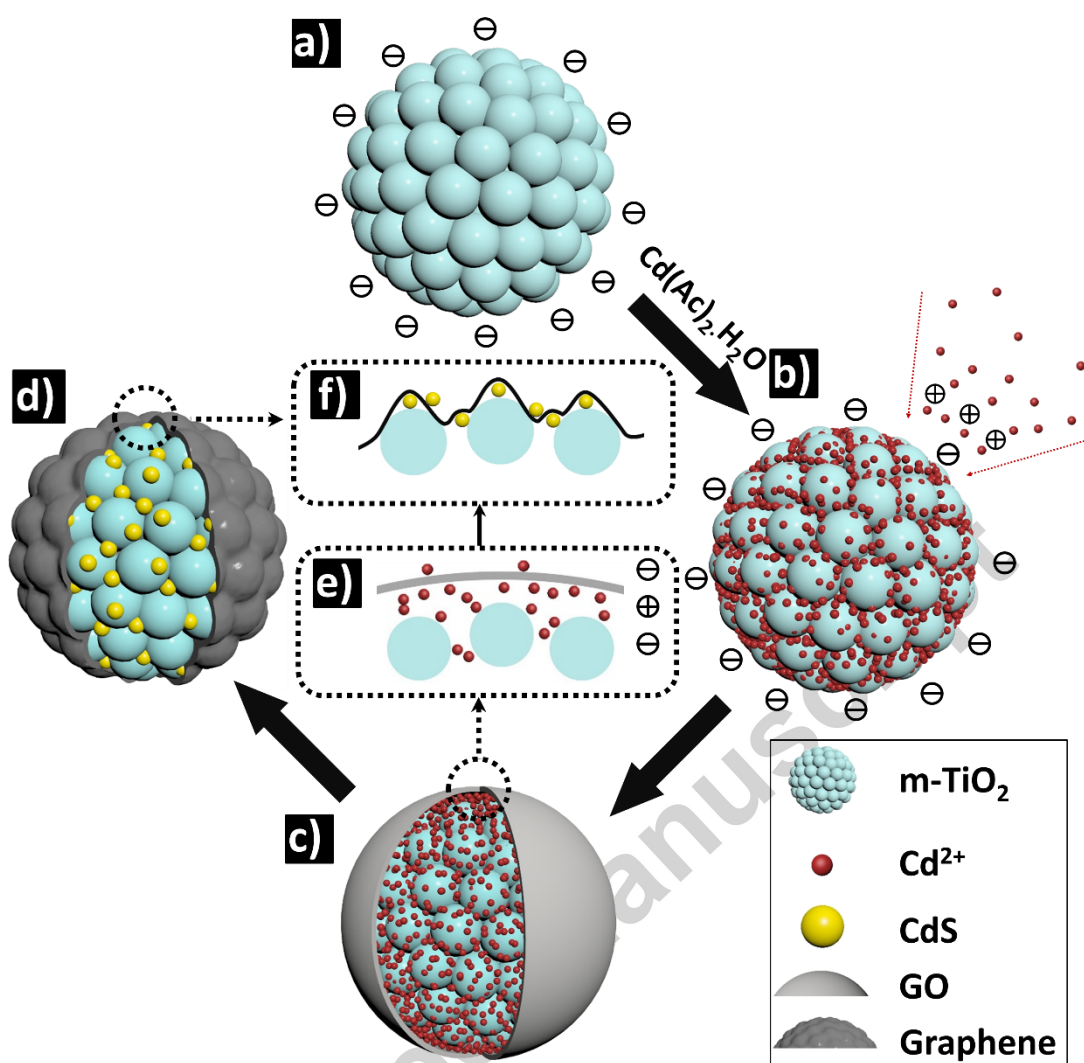


Fig. 1. Scheme illustrating the Negative-Positive-Negative hierarchical electrostatic assembly synthesis of CdS/m-TiO₂/G. a) m-TiO₂ bead with negatively charged surface in DMSO solution. b) Formation of an electronic-bi-layer after absorption of Cd²⁺ onto TiO₂. c) Hierarchical m-TiO₂/GO core-shell structure filled Cd²⁺ after adding the graphene oxide nanosheets. d) Hierarchical CdS/m-TiO₂/G after solvothermal treatment for the formation of CdS and chemical reduction of GO. e) Ionic interactions proposed during the formation of the hierarchical m-TiO₂/GO filled with Cd²⁺. (f) Formation and well-dispersion of CdS in the hierarchical CdS/m-TiO₂/G structure.

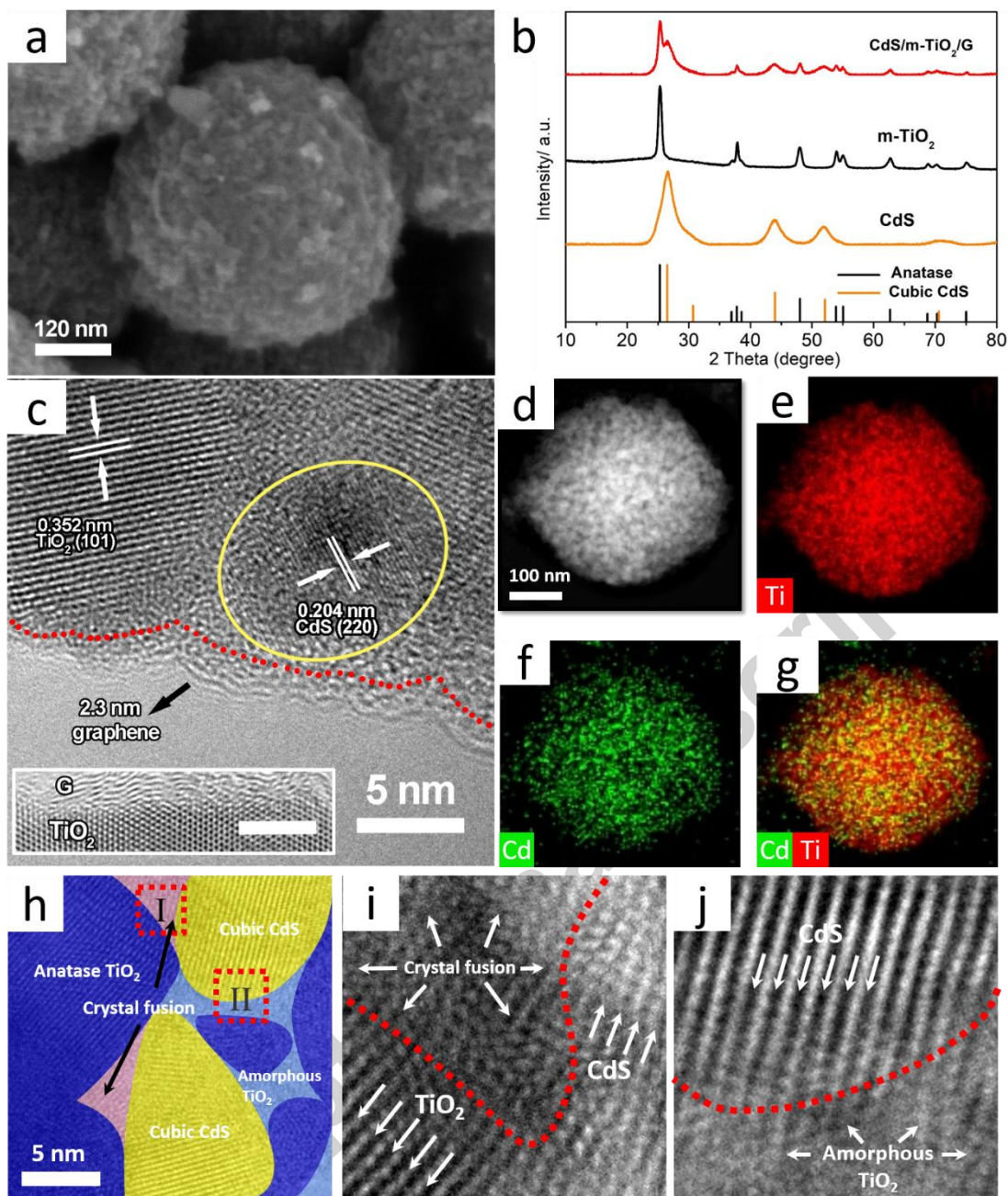


Fig. 2. a) SEM image of CdS/m-TiO₂/G, coated with graphene sheets. b) XRD patterns of CdS, m-TiO₂ and CdS/m-TiO₂/G. c) The HRTEM image of CdS/m-TiO₂/G, the inset (taken from Fig. S2) shows the interface between TiO₂ nanocrystal and graphene (G), and the scale bar represents 5 nm. d-g) HAADF-STEM image and EDS elemental maps of CdS/m-TiO₂/G. h) HRTEM image of nanocrystalline domains of anatase TiO₂, CdS, amorphous TiO₂, and heterojunction, and four different colors are used to distinguish the different phases. i) Inverse FFT image of region I, showing crystal fusion region between TiO₂ and CdS, and j) inverse FFT image of region II, showing nanocrystalline domains of CdS and amorphous TiO₂.

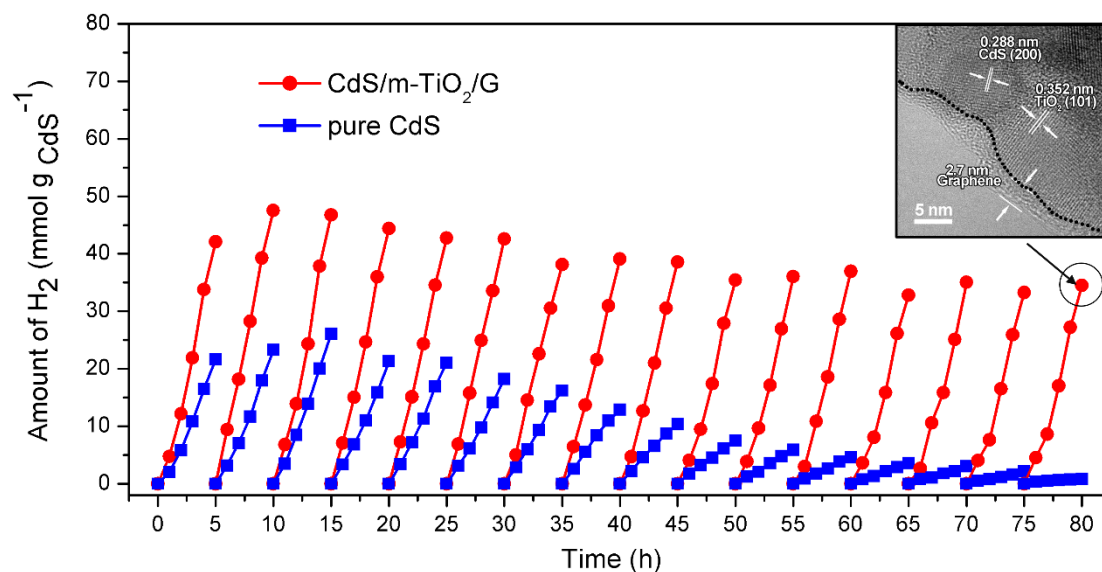


Fig. 3. Photostability for the H₂ production of CdS/m-TiO₂/G and CdS under visible light irradiation (≥ 420 nm), and the sacrificial reagent containing 0.1 M Na₂SO₃ and 0.1 M Na₂S aqueous solution is added only once during the whole photocatalytic reaction; The inset shows a HRTEM image of CdS/m-TiO₂/G after the 80 h photocatalytic H₂ production test.

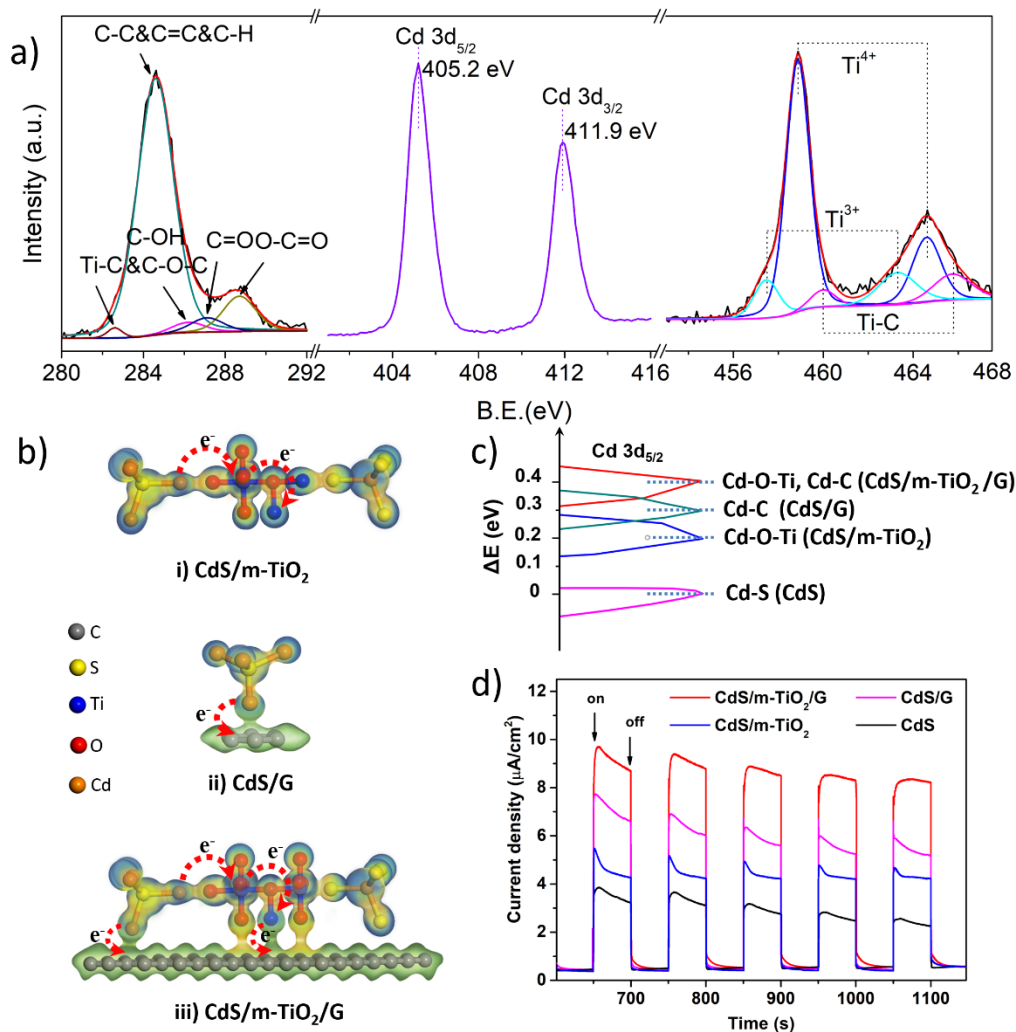


Fig. 4. a) XPS spectra of CdS/m-TiO₂/G. b) New generated bond models at the interface between different phases. i~iii) Proposed geometric structures of the newly formed chemical bonds in the binary nanostructured photocatalysts and the ternary nanostructured photocatalyst. The three-dimensional electron cloud is proposed by colored bubbles, and the red dotted lines simulate the photogenerated electron transfer paths during the photocatalytic reaction. c) Cd 3d_{5/2} chemical shift among m-TiO₂, CdS, CdS/G, CdS/m-TiO₂ and CdS/m-TiO₂/G. d) Transient photocurrent responses of CdS, CdS/G, CdS/m-TiO₂ and CdS/m-TiO₂/G in a 0.5 M Na₂SO₄ aqueous solution at 0.5 V vs. Ag/AgCl under visible light irradiation (λ ≥ 420 nm).

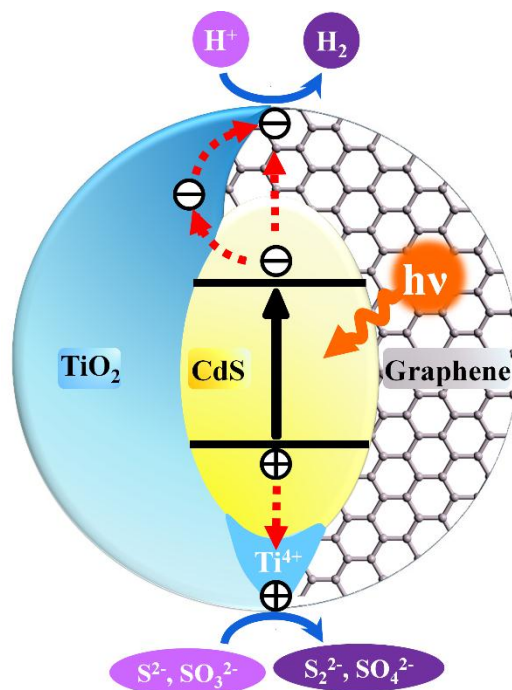
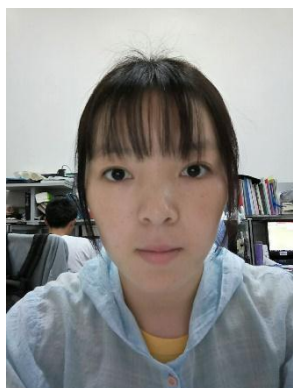


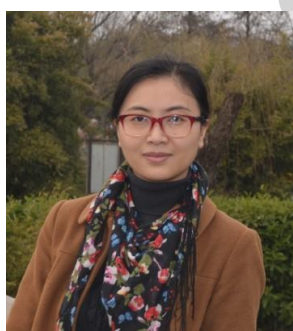
Fig. 5. Schematic description of the transfer and separation of the photogenerated electrons and holes in the CdS/m-TiO₂/G structure.

Vitae

Yi Lu is currently a PhD candidate under the supervision of Prof. Xiao-Yu Yang and Prof. Baolian Su from the State Key Laboratory of Advanced Technology for Materials Synthesis and Processing at Wuhan University of Technology, China. His research interest is focused on design and synthesis of graphene-based composite, as well as their applications in energy and environmental fields.



Xiu Cheng received his B. S. degree from Wuhan University of Technology in 2016, she is now pursuing his M.S. degree under the supervision of Prof. Xiao-Yu Yang and Her research interests mainly focus on titania composite photocatalytic materials.



Dr. Ge Tian earned her B.S. degree from Jilin University in 2001 and her Ph. D. degree from Jilin University, China in 2006. She is currently working at school of materials science at WHUT. Her research is aimed at nanostructured materials, crystalline materials, hybrid materials, catalysis, and cell-surface-engineering.



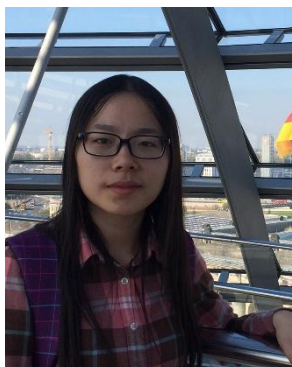
Heng Zhao received his Bachelor degree from Wuhan University of Technology majored in Applied Chemistry in 2013. He is currently a Ph.D. student in Wuhan University of Technology majored in Material Physics and Chemistry under guidance of Prof. Yu Li and Prof. Bao-Lian Su. His research mainly focuses on the design and synthesis of three-dimensionally ordered macroporous catalysts for the photocatalytic hydrogen generation.



Li He received her B. S. degree from Wuhan University of Technology in 2017, she is now pursuing his M.S. degree under the supervision of Prof. Xiao-Yu Yang and Her research interests mainly focus on nanomaterials for energy storage and photocatalytic materials.



Jie Hu received her B. S. degree from Wuhan University of Technology in 2011. She is currently a Ph.D. student in Wuhan University of Technology majored in Material Physics and Chemistry under guidance of Prof. Xiao-yu Yang and Prof. Bao-Lian Su. Her research mainly focuses on the design and synthesis of hierarchical porous photocatalysts.



Si-Ming Wu received her B. S. degree from Wuhan University of Technology in 2013. She is now pursuing her Ph.D. under the supervision of Prof. Xiao-Yu Yang in Wuhan University of Technology. Her research mainly focuses on the design, synthesis and application of hierarchically porous materials



Dr. Ying Dong is a post-doctoral researcher in the group of Prof. Xiao-Yu Yang at State Key Laboratory Advanced Technology for Materials Synthesis and Processing, Wuhan University of Technology. She received her Ph.D. in 2015 from Lanzhou Institute of Chemical Physics, Chinese Academy of Sciences. Her current research interests mainly focus on design, fabrication and characterization of graphene-based materials and their applications in the fields of environment remediation and energy conversion and storage.



Dr. Gang-Gang Chang received his PhD degree (2016) in applied chemistry from Zhejiang University under the direction of Prof. Qilong Ren, and joined Prof. Banglin Chen's group as a visiting scholar at the University of Texas at San Antonio during 2015~2016. Now he is working at Wuhan University of Technology as an associate professor in the department of chemical engineering. His current research interests are porous materials for chemical separation and heterogeneous catalysis.



Prof. Silvia Lenaerts studied Chemistry at KULeuven from 1984 to 1988. After a short research interval at UHasselt, she worked on a PhD concerning gas sensors for NO_x, CO and C_xH_y detection at IMEC and KULeuven. Since 2006 she is engaged at the Universiteit Antwerpen, first as a research manager, later on as professor and as head of the department of bioscience engineering. She teaches environmental chemistry, catalysis, applied thermodynamics, biosphere-air and other courses. She is the founder and spokesman of the research group "sustainable energy and air purification", which momentarily counts around 18 researchers.



Prof. Stéphane Siffert received his PhD degree in chemistry from Dr F. Garin's catalysis group at the University of Strasbourg. After working at the University of Namur as a post-doctoral researcher in Prof. Bao-Lian Su's group, he joined the University of Littoral in 1998 and has been a professor since 2007. His group is working on catalysis treatment and clean energy. He has published more than 75 articles in peer reviewed journals.



Prof. Van Tendeloo studied physics and graduated from the University of Antwerp (Belgium) in 1974. He is a professor at the University of Antwerp. His research focuses on the application of electron microscopy to different aspects of materials science. He is the head of the electron microscopy group EMAT and director of the Nano Center of Excellence of the University. In 2009, he received an ERC Advanced Grant (COUNTATOMS).



Ling-Ling Xu received her B.S. and Ph.D. degrees majoring in Biomedical engineering from Huazhong University of Science and Technology in 2008 and 2013. She is currently an engineer in National Center for Magnetic Resonance at Chinese Academy of Sciences in Wuhan. Her research focuses on the developments and applications of optical microscopy.



Dr. Zhao-Fei Li received his B.S. degree and PhD degree in Inorganic Chemistry from Peking University, China in 2000 and 2005, respectively. He worked as a postdoctoral researcher at Ruhr-University Bochum in Germany from 2005 to 2007. Then he worked as a research associate in Tohoku University and assistant professor at Kyoto University in Japan. He joined the Petrochemical Research Institute of PetroChina in China as a senior Engineer since 2010. His current research interests include the preparation and application of inorganic porous materials, porous alumina, FCC catalysts and related materials.



Prof. Xiao-Yu Yang received his Ph.D. from Jilin University (co-educated at the University of Namur, Belgium). After a postdoctoral fellowship at the FUNDP, he worked as a “Chargé de Recherches” at the National Foundation of Scientific Research in Belgium. He is currently working as full professor at State Key Laboratory of Advanced Technology for Material Synthesis and Processing at Wuhan University of Technology in 2010. His research is aimed at new synthesis pathways towards novel porous systems, catalysts, bio-nanoreactors, bio-inspired materials and biofuel cells.



Prof. Bao-Lian Su created the Laboratory of Inorganic Materials Chemistry (CMI) at the University of Namur, Belgium in 1995. He is currently Full Professor of Chemistry, Member of the Royal Academy of Belgium, Fellow of the Royal Society of Chemistry. He is also Changjiang Professor at Wuhan University of Technology and an “Expert of the State” in the frame of “Thousands Talents” program, China. His current research fields include the synthesis, hierarchically porous and bio-inspired materials, living materials and leaf-like materials and the immobilization

of bio-organisms for artificial photosynthesis, catalysis, energy conversion and storage, biotechnology, cell therapy and biomedical applications.

Research highlights

A hierarchical CdS/mesoporous TiO₂/graphene ternary photocatalyst has been successfully prepared via electric-triple-layer hierarchical synthesis.

The ternary photocatalyst exhibits an extremely high H₂ production rate and long-term photostability.

The ternary nanojunction effect of the hierarchical CdS/m-TiO₂/G has been investigated from orbitals hybrid, bonding energy to atom-stress distortion and nano-interface fusion.

Accepted manuscript